ELSEVIER

Journal of Alloys and Compounds 403 (2005) 239–244

Journal of ALLOYS AND COMPOUNDS

www.elsevier.com/locate/jallcom

Effect of Nb content on the microstructure and mechanical properties of Zr–Cu–Ni–Al–Nb glass forming alloys

Y.F. Sun [a], C.H. Shek [b,*], B.C. Wei [c], W.H. Li [c], Y.R. Wang [c]

[a] *Research Center for Materials, Department of Materials Science and Engineering, Zhengzhou University, Zhengzhou 450002, China*
[b] *Department of Physics and Material Science, City University of Hong Kong, 83 Tat Chee Avenue, Kowloon Tong, Hong Kong, China*
[c] *National Microgravity Lab, Institute of Mechanics, Chinese Academy of Sciences, Beijing 100080, China*

Received 22 February 2005; received in revised form 31 May 2005; accepted 2 June 2005
Available online 27 July 2005

Abstract

$(Zr_{65}Al_{10}Ni_{10}Cu_{15})_{100-x}Nb_x$ glass forming alloys with Nb contents ranging from 0 to 15 at.% were prepared by water-cooled copper mould cast. The alloys with different Nb contents exhibited different microstructures and mechanical properties. Unlike the monolithic $Zr_{65}Al_{10}Ni_{10}Cu_{15}$ bulk metallic glass, only a few primary bcc β-Ti phase dendrites were found to distribute in the glassy matrix of the alloys with $x = 5$. For alloys with $x = 10$, more β-phase dendrites forms, together with quasicrystalline particles densely distributed in the matrix of the alloys. For alloys with $x = 15$, the microstructure of the alloy is dominated by a high density of fully developed β-phase dendrites and the volume fraction of quasicrystalline particles significantly decreases. Room temperature compression tests showed that the alloys with $x = 5$ failed at 1793 MPa and exhibited an obvious plastic strain of 3.05%, while the other samples all failed in a brittle manner. The ultimate fracture strengths are 1793, 1975 and 1572 MPa for the alloys with $x = 0$, 10 and 15 at.% Nb, respectively.

Keywords: Bulk metallic glass; Composites; Shear bands; Microstructure

1. Introduction

Since the first emergence of bulk metallic glass (BMG) some 40 years ago, a large number of multicomponent metallic glass alloys with strong glass forming ability (GFA) and high thermal stability have been synthesized. In spite of their metallic bonding, the deformation behavior of BMGs differs greatly from those of their crystalline counterpart due to the absence of long-range order in the atomic arrangement. Nearly all the BMGs discovered so far exhibit shear localization under loading at room temperature, leading to catastrophic shear failure immediately after yielding under unconstrained conditions [1–5]. With a purpose to improve the plasticity of BMG, the development of BMG matrix composites has attracted lots of attentions recently. Among the composites, those with a microstructure of ductile dendrites and glassy/nanocrystalline matrix seem to be most promising [6–9]. The BMG matrix composites with such a microstructure often exhibit a high fracture strength combined with improved global plasticity. Upon loading, the ductile dendritic phase acts to seed the initiation of organized shear band patterns, and to confine the propagation of individual shear bands by the interaction between the dendrite and the nucleated shear bands. This hinders a single shear band to extend critically through the whole sample at the onset of plastic deformation and therefore plasticity is distributed more homogeneously in the shear band patterns, which result in high strains to failure and an apparent work hardening behavior of the materials [10,11].

Recently, Hays et al. developed Zr–Ti–Nb–Cu–Ni–Be BMG composites by coupling a high-strength glassy phase with ductile dendritic bcc β-Ti phase, which significantly improves the deformation behavior of the composites and displays a plastic strain of 6–7% [11–13]. Shortly after this, Kuhn et al. developed a series of ductile β-Ti dendrites

* Corresponding author. Tel.: +852 27887798; fax: +852 27887830.
E-mail address: apchshek@cityu.edu.hk (C.H. Shek).

0925-8388/$ – see front matter © 2005 Elsevier B.V. All rights reserved.
doi:10.1016/j.jallcom.2005.06.006

reinforced Be-free Zr-based BMG matrix composites with a plastic strain in the range of 0.6–14.8% [6,14]. Up to now, some Zr-based and Ti-based BMG matrix composites exhibiting such a microstructure of ductile dendrites and glassy/nanocrystalline matrix have been successfully synthesized. However, it is difficult to synthesize BMG matrix composites reinforced solely with dendritic β-phase simply by modifying the original BMG composition, because the formation of β-phase lies in a narrow composition range. The glass forming alloys usually have more than five constituents, between which intermetallic compounds can easily form [15]. Therefore, the attempt to synthesize the composites with such a dendrite/amorphous microstructure often lead to the formation of dendritic phase together with other intermetallic compounds or quasicrystalline particles, which will deteriorate the mechanical properties due to their intrinsic brittleness. Meanwhile, it is noted that the casting conditions also have an important effect on the microstructure of the composites, and subsequently affect their mechanical properties [6,14].

In this paper, $(Zr_{65}Al_{10}Ni_{10}Cu_{15})_{100-x}Nb_x$ glass forming alloys with different microstructure were prepared by adjusting the Nb content in the range from 0 to 15 at.%. The phase constituent, microstructural evolution and room temperature mechanical properties of the alloys were investigated.

2. Experimental procedure

Four different master alloy ingots with compositions of $Zr_{65}Al_{10}Ni_{10}Cu_{15}$ (alloy A), $(Zr_{65}Al_{10}Ni_{10}Cu_{15})_{95}Nb_5$ (alloy B), $(Zr_{65}Al_{10}Ni_{10}Cu_{15})_{90}Nb_{10}$ (alloy C) and $(Zr_{65}Al_{10}Ni_{10}Cu_{15})_{85}Nb_{15}$ (alloy D) were prepared by arc melting pure Zr, Al, Ni, Cu and Nb under a Ti-gettered argon atmosphere. For getting a homogeneous master alloy, Nb, which has a much higher melting point compared with the other four elements, and Zr were first arc melted to produce an intermediate binary Zr–Nb alloy. The master alloys were then made by arc melting the mixture of the intermediate alloy and the other pure metals. From these master alloys, alloy rods with 3 mm in diameter and 70 mm in length were prepared by suction casting into a water-cooled copper mold.

The phase constitutions of the as-cast alloys were analyzed by X-ray diffraction (XRD) using a Siemens D 500/501 diffractometer with Cu Kα radiation. The thermal stability of all samples was assessed by differential scanning calorimetry (DSC) in a Perkin-Elmer DSC7 with flowing argon atmosphere and a heating rate of 20 K/min. The microstructures of the alloys were examined with scanning electron microscopy (SEM) and energy dispersive X-ray spectroscopy (EDXS) using a Jeol 5200 SEM and Oxford energy dispersive X-ray spectrometer, respectively. Transmission electron microscopy (TEM) was carried out with a Philips TECNAI 20 electron microscope, operating at 200 kV. The TEM samples were first mechanically ground to a 30 μm thick plate and then twin-jet electropolished using a solution mixed in the ratio $HF:HClO_4:CH_4O = 1:1:9$. Room temperature uniaxial compression tests were conducted under quasistatic loading (strain rate of 1×10^{-4}) with an Instron 8852 device, which has an axial stiffness of 100 kN/mm and a strain measurement accuracy of 0.05% of full scale and 0.5% of reading. Samples with an aspect ratio of about 2:1 were used for the compression tests.

3. Results and discussions

The XRD patterns of the as-cast $(Zr_{65}Al_{10}Ni_{10}Cu_{15})_{100-x}Nb_x$ glass forming alloys are shown in Fig. 1. For alloys A and B, a typical broad hump was observed with no visible crystalline diffraction peak, indicating that these as-cast samples were fully amorphous. On the other hand, there are some obvious crystalline diffraction peaks on the XRD curve of alloys C and D. Similar to the Be-free Zr-based BMG composites reinforced with bcc ductile dendrites [15], alloys C and D in this paper have bcc β-Ti phase precipitated from the amorphous matrix and the simultaneous appearance of quasicrystalline phase, which is also verified by microstructure characterization discussed in a later section. From the XRD pattern, the diffraction peak of quasicrystalline phase of alloy C are relatively stronger in intensity than that of alloy D. It indicates that the nucleation and growth of quasicrystalline phase is suppressed with increasing Nb contents and the bcc β-phase will form preferentially. Some additional reflections resembling the pattern of a phase with $Zr_{73}Cu_{14}Al_{13}$ composition but unknown structure was also found in the XRD pattern of alloy D [14].

Fig. 2 shows the DSC scans for the as-cast $(Zr_{65}Al_{10}Ni_{10}Cu_{15})_{100-x}Nb_x$ alloys. A distinct glass transition with an supercooled liquid region can be observed in each individual sample. From the DSC scans, the glass transition temperature T_g increases and the undercooled liquid region decreases with increasing Nb contents. For alloys A and B, there is only one exothermic peak during the heating process, while more

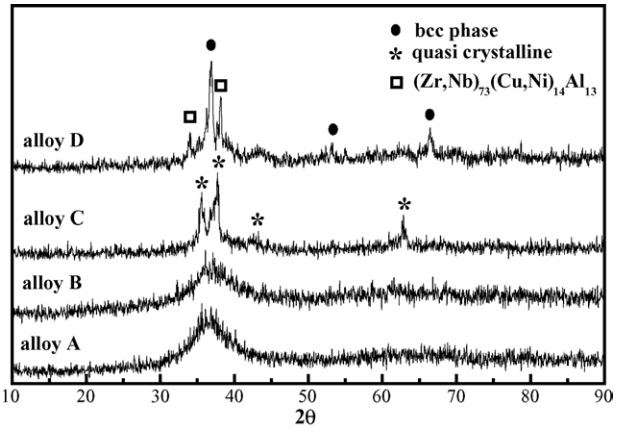

Fig. 1. X-ray diffraction pattern for the as-cast $(Zr_{65}Al_{10}Ni_{10}Cu_{15})_{100-x}Nb_x$ alloys.

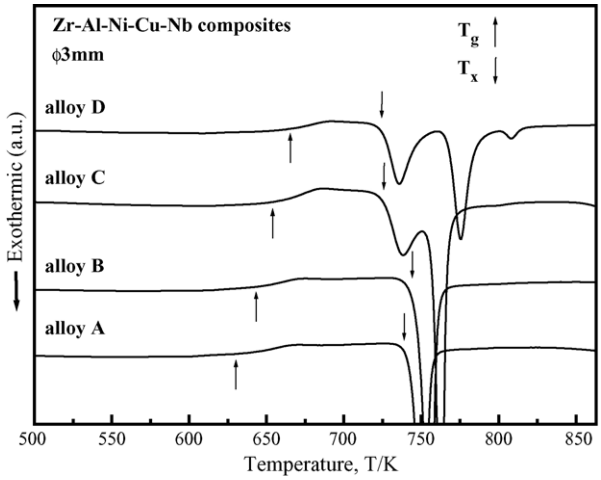

Fig. 2. DSC scans for the as-cast $(Zr_{65}Al_{10}Ni_{10}Cu_{15})_{100-x}Nb_x$ alloys.

exothermic peaks can be seen from the DSC curve of alloys C and D. Since there was metastable quasicrystalline phase formed in the two later samples, the additional exothermic event is therefore the extra phase transformation related to the quasicrystalline phase before the primary crystallization.

Fig. 3 shows the SEM images of the polished and etched cross-sections of the $(Zr_{65}Al_{10}Ni_{10}Cu_{15})_{100-x}Nb_x$ alloys. No obvious crystalline precipitate is observed in the homogeneous amorphous matrix of alloy A, as shown in Fig. 3(a). Fig. 3(b) shows the image of the alloy B, a few dendritic precipitates can be seen at the center of some of the dark gray areas. The size of the dendritic phase is about 10 μm and the primary dendrite arm can be seen. However, the volume fraction of the small sized dendrites is too small to be detected by XRD. For alloy C, about 100 μm thick fully glassy shell was found in the outermost region of the alloy rods. Some

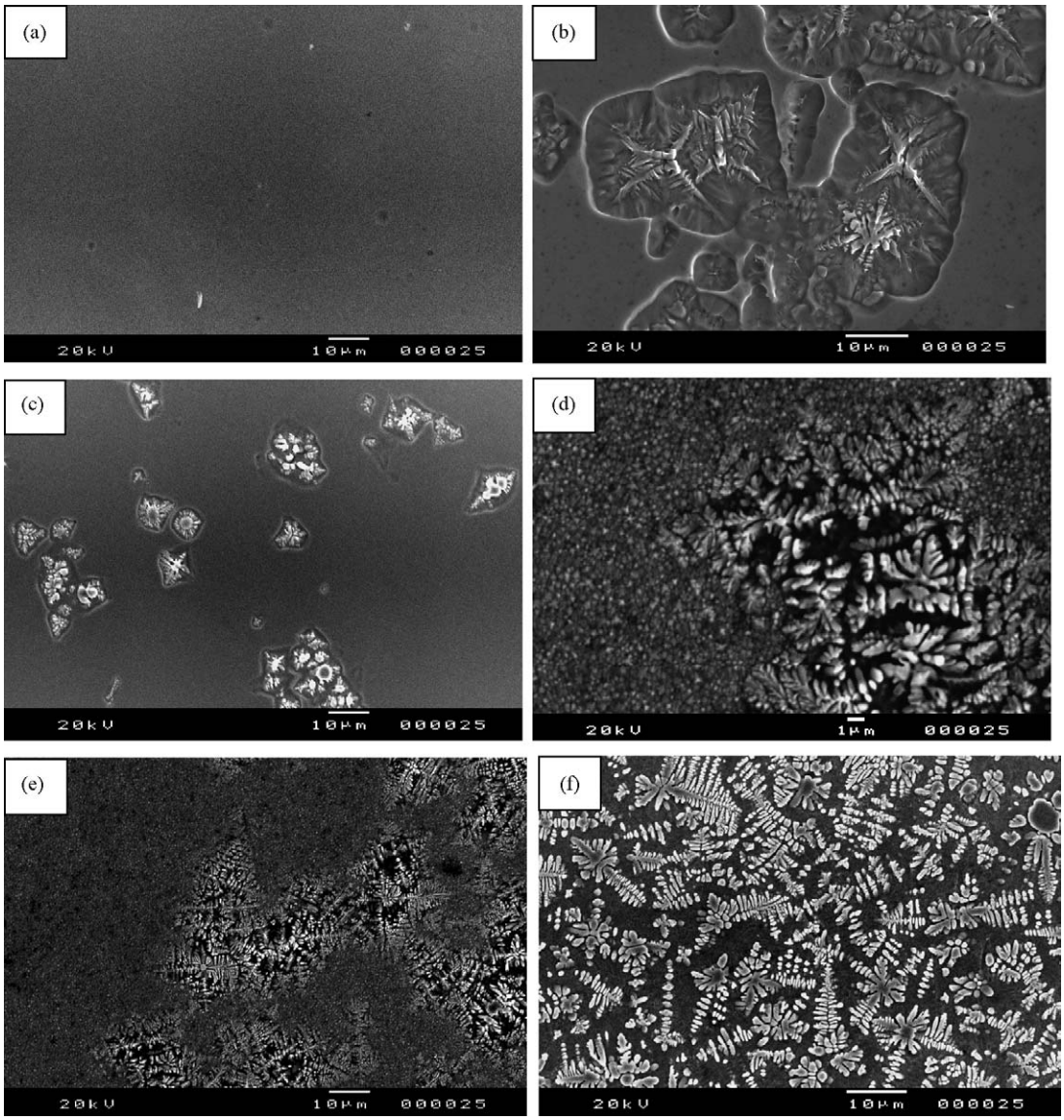

Fig. 3. SEM images of the cross-section of the as-cast $(Zr_{65}Al_{10}Ni_{10}Cu_{15})_{100-x}Nb_x$ alloys: (a) alloy A; (b) alloy B; (c) alloy C; (d) alloy C; (e) alloy D; (f) alloy D.

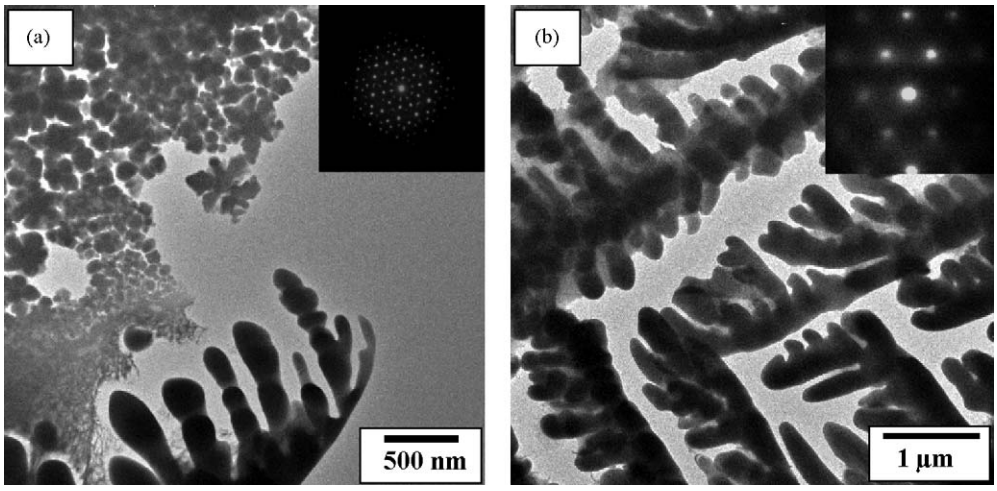

Fig. 4. TEM image and SAED pattern of the (a) quasicrystalline and dendritic phase in alloy C with five-fold symmetry SAED pattern inset; (b) bcc phase in alloy D with SAED pattern taken along [1 1 1] zone inset.

dendrites form at the center of the sample rod, as shown in Fig. 3(c). Fig. 3(d) shows the dendrites at higher magnification, dense particles can be found around the developing dendrites. Fig. 4(a) is the TEM image of the dense particles and the dendritic phase. The corresponding selected area electron diffraction (SAED) pattern of the particles is also shown as an inset. The five-fold symmetry of the diffraction pattern corroborates the formation of quasicrystalline phase. A fully glassy shell of about 100 μm thick was also found in the outermost regions of the alloy D rods. Going deeper from the shell, a 200 μm thick region with a microstructure of quasicrystalline particles and dendrite phase, which is similar to that of alloy C, can be found in Fig. 3(e). Towards the center of the sample rod, the microstructure is dominated by a high density of the dendrite phase distributed in the matrix, as shown in Fig. 3(f). The dendrite structure has primary dendrite axes with length of 10–20 μm and a radius of about 500 nm. The composition of the dendrite phase is about 60.8 at.% Zr, 6.7 at.% Al, 3.4 at.% Ni, 7.2 at.% Cu and 21.9 at.% Nb, while that of the matrix is about 48.8 at.% Zr, 12.2 at.% Al, 14.16 at.% Ni, 19.23 at.% Cu and 5.43 at.% Nb. It reveals that the composition of the dendrite phase strongly deviate from the nominal composition. This phase is depleted in Ni and enriched in Zr and Nb. The highest Nb content of the β-phase can reach about 21.9 at.%, which is much higher than that of the β-phase in other Zr-based composites [14,16]. Fig. 4(b) is the TEM image and the SAED pattern of the dendrite phase. The SAED pattern taken along the [1 1 1] zone axis corroborates the formation of a bcc phase.

A series of mechanical tests were conducted on the as-cast alloys with different Nb contents. Fig. 5 shows the typical uniaxial compressive stress–strain curves, in which the origins of the curves have been displaced for clarity. Except for alloy B, all the other samples exhibit brittle fracture but with different fracture strength. The fracture strength for alloys A, C and D are about 1793, 1975 and 1572 MPa, respectively. However, alloy B exhibits initial elastic deformation, followed by yielding, plastic deformation and finally fracture under compressive loading. The serrated flow can be clearly seen on the stress–strain curve in Fig. 5(b). The samples exhibit yield strength of 1793 MPa and fracture strength of 1713 MPa, which reveals some work softening during the end of the deformation process. The total plastic strain of the sample is about 3.05%.

With different Nb content, the as-cast $(Zr_{65}Al_{10}Ni_{10}Cu_{15})_{100-x}Nb_x$ alloys exhibit different fracture feature. Fig. 6 shows the fracture surfaces of alloys B, C and D. The compressive failure of alloys A and B all took place along the maximum shear plane, which was inclined by about 45° to the direction of the compressive load. Fig. 6(a) shows the profile of the lateral surface near the fracture plane of alloy B. Branching of the slip bands can been clearly seen. The slip bands formed before branching can be called the pri-

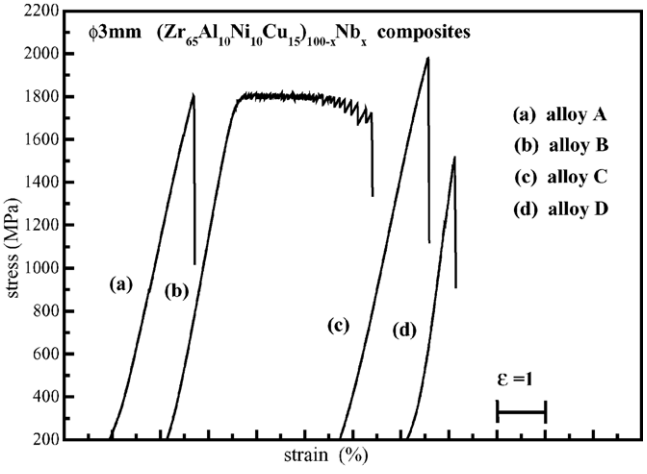

Fig. 5. Room temperature compressive stress–strain curves of the as-cast $(Zr_{65}Al_{10}Ni_{10}Cu_{15})_{100-x}Nb_x$: (a) alloy A; (b) alloy B; (c) alloy C; (d) alloy D.

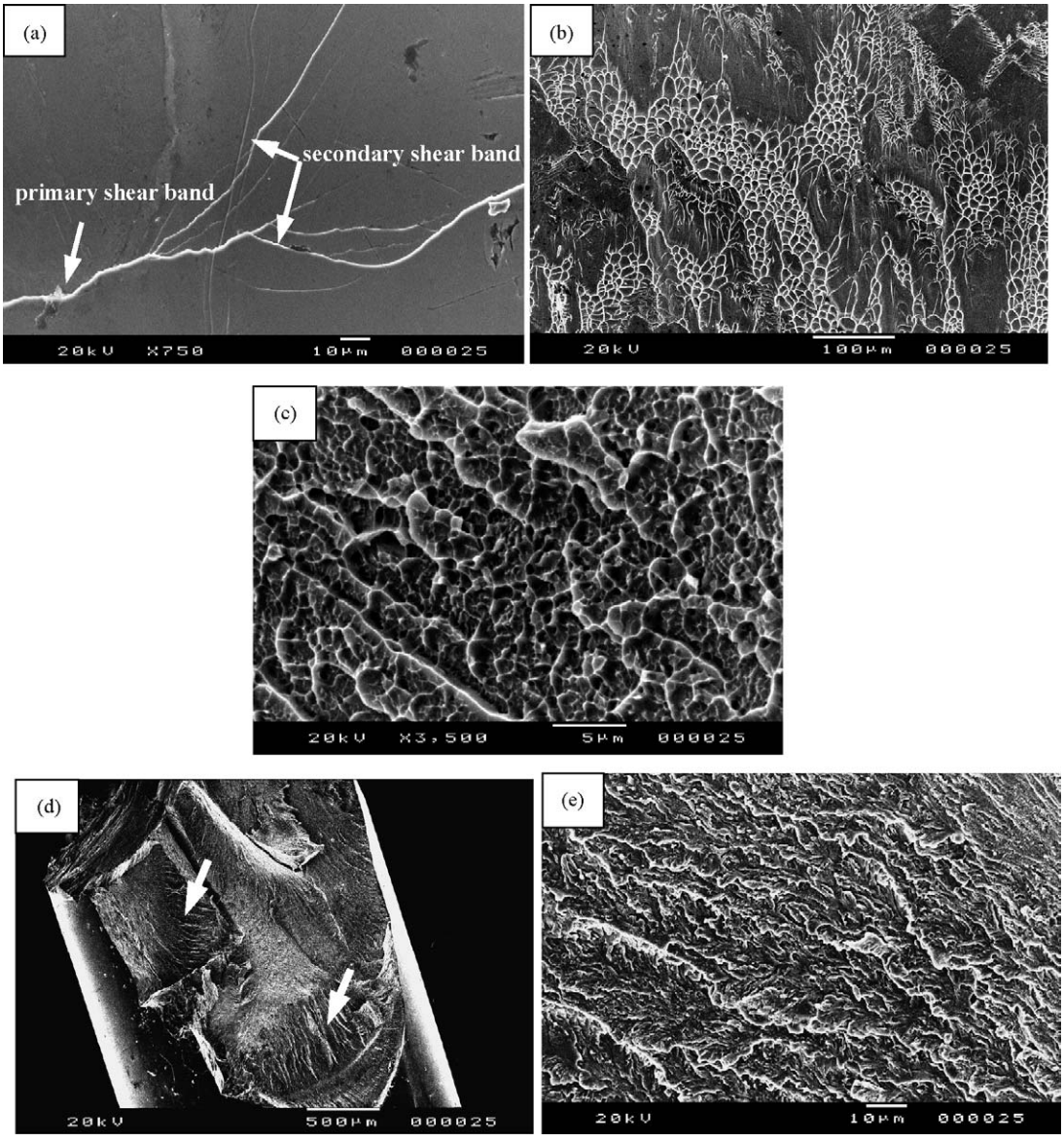

Fig. 6. Fractography of as-cast $(Zr_{65}Al_{10}Ni_{10}Cu_{15})_{100-x}Nb_x$ alloy shows: (a) the sample surface near fracture plane, alloy B; (b) fracture surface, alloy B; (c) fracture surface, alloy C; (d) fracture geometry, alloy D and (e) fracture surface, alloy D.

mary slip bands, while the slip bands after branching can be called the secondary slip bands. Lin et al. has studied the enhanced plastic strain in Zr-based BMG and believed that the slip bands forming in groups is due to the branching of individual shear bands as they propagate through the material [17]. However, no obvious slip bands can be found on the lateral surface of other as-cast alloys. Fig. 6(b) shows the morphology of the fracture surface of alloy B. A substantial portion of the fracture surface has a vein pattern that extends along the maximum shear stress direction. The vein patterns are more branched and the branching presumably redistributes plastic strain or diverse the stress into different shear plane. The resultant shear strain in any one branch thus may be much smaller than that of a single, unbranched shear band. This makes it more difficult for a propagating shear band to nucleate a crack that will cause failure. The fracture was thus retarded and shows significant plastic strain before failure.

For alloy C, the fracture surface shown in Fig. 6(c) exhibits a honeycomb-like morphology, which was formed via peeling-off of the quasicrystalline particles. The deformation behavior shows high strength but brittle fracture at room temperature, which is typical for quasicrystalline materials [18].

The overall profile of the fracture surface of alloy D is shown in Fig. 6(d). There are different fracture planes on the fracture surface. The arrows show the interactions of the deformation bands indicating inhomogeneous deformation during the fracture. Fig. 6(e) shows the morphology of the center part of the fracture surface. No vein patterns were

found and the fracture surface reveals typical brittle features. It was reported that the bcc dendrites is unstable against shear and has a very low shear modulus of 22.7 GPa [10]. The dendrites deformed via plastic deformation mechanisms such as dislocation motion and twining, which contribute to the plastic strain and initiate shear bands, while the matrix provides high strength. Therefore, the higher the volume fraction of the dendrite phase, the larger is the plastic strain. However, the plasticity does not occur for this alloy [19]. The embitterment of the as-cast alloys might be caused by the microstructure difference between the center part and the peripheral part of the materials.

4. Conclusion

The microstructure, mechanical properties and fracture features of as-cast $(Zr_{65}Al_{10}Ni_{10}Cu_{15})_{100-x}Nb_x$ alloys with different Nb contents are investigated. The following conclusions can be made:

(1) The glass transition temperature slightly increased and the supercooled liquid region decreased with increasing Nb content. For alloys with 10 and 15 at.% Nb, the DSC curves exhibit more than one exothermic peak due to the precipitation of quasicrystalline phase.
(2) The microstructure varied greatly due to different Nb contents. In alloy B (5 at.% Nb), apart from the fully amorphous structure some dendrite phases with very small size, which could not be detected by XRD, were found. Quasicrystalline phase with the size of less than 200 nm was the dominant constituent in alloy C (10 at.% Nb), while some bcc phase was also formed. Though there was some quasicrystalline phase near the sample surface of alloy D (15 at.% Nb), the bcc phase was the dominant phase, which was fully developed with the size of about 15 μm.
(3) Among the four alloys, only alloy B (5 at.% Nb) exhibited plastic deformation with about 3.05% of plastic strain prior to fracture. The improved plasticity is due to the branching of the shear bands. The other three alloys failed in brittle fracture manner under the compression test. The ultimate compression stresses of the four alloys are of 1793, 1793, 1975 and 1572 MPa, respectively.

Acknowledgments

This work was supported by a City University of Hong Kong Strategic Research Grant (Project number: 7001529), National Natural Science Foundation of China (Grant number: 50101012) and Knowledge Innovation Program of Chinese Academy of Sciences (Project number: KJCX2-SW-L05).

References

[1] C. Gilbert, R.O. Ritchie, W.L. Johnson, Appl. Phys. Lett. 71 (1997) 476.
[2] K. Kawamura, H. Kato, A. Inoue, Appl. Phys. Lett. 67 (1995) 2008–2010.
[3] C.T. Liu, L. Heatherly, D.S. Easton, Metall. Mater. Trans 29A (1998) 1811–1820.
[4] H. Choi-Yim, W.L. Johnson, Appl. Phys. Lett. 71 (1997) 3808–3810.
[5] C. Fan, D.V. Louzguine, C.F. Li, A. Inoue, Appl. Phys. Lett. 75 (1999) 341–434.
[6] J. Eckert, U. Kuhn, N. Mattern, Intermetallics 10 (2002) 1183–1190.
[7] H. Choi-Yim, R.D. Conner, F. Szuecs, W.L. Johnson, Acta Mater. 50 (2002) 2737–2748.
[8] Q.L. Dai, B.B. Sun, M.L. Sui, J. Mater. Res. 19 (2004) 2557–2569.
[9] G. He, J. Eckert, W. Löser, L. Schultz, Nat. Mater. 2 (2003) 33–38.
[10] F. Szuecs, C.P. Kim, W.J. Johnson, Acta Mater. 49 (2001) 1507–1513.
[11] C.C. Hays, C.P. Kim, W.L. Johnson, Phys. Rev. Lett. 84 (2000) 2901–2904.
[12] C.C. Hays, C.P. Kim, W.L. Johnson, Mater. Sci. Forum 343 (2002) 191–196.
[13] C.C. Hays, C.P. Kim, W.L. Johnson, Mater. Sci. Eng. 304 (2001) 650–655.
[14] J. Das, W. Loser, U. Kuhn, Appl. Phys. Lett. 82 (2003) 4690–4692.
[15] G. He, W. Loser, J. Eckert, Mater. Sci. Eng. A352 (2003) 179–185.
[16] U. Kuhn, J. Eckert, N. Mattern, Appl. Phys. Lett. 80 (2002) 2478–2480.
[17] L.Q. Xing, Y. Li, K.T. Ramesh, Phys. Rev. B 64 (2001), 180201-1.
[18] A. Leonhard, L.Q. Xing, M. Heilmaier, Nanostruct. Mater. 10 (1998) 805–816.
[19] G. He, W. Loser, J. Eckert, Metall. Mater. Trans. 35A (2004) 1591–1601.